ISSN 0023-1584, Kinetics and Catalysis, 2011, Vol. 52, No. 6, pp. 843–850. © Pleiades Publishing, Ltd., 2011.
Original Russian Text © T.N. Afonasenko, D.A. Shlyapin, N.N. Leont'eva, T.I. Gulyaeva, K.S. Buyal'skaya, M.V. Trenikhin, P.G. Tsyrul'nikov, 2011, published in Kinetika i Kataliz, 2011, Vol. 52, No. 6, pp. 864–872.

Selective Oxidation of Carbon Monoxide in Hydrogen-Containing Gas on $CuO–CeO_2/Al_2O_3$ Catalysts Prepared by Surface Self-Propagating Thermal Synthesis

T. N. Afonasenko, D. A. Shlyapin, N. N. Leont'eva, T. I. Gulyaeva, K. S. Buyal'skaya, M. V. Trenikhin, and P. G. Tsyrul'nikov

Institute of Hydrocarbon Processing, Siberian Branch, Russian Academy of Sciences, Omsk, 644040 Russia

e-mail: atnik@ihcp.oscsbras.ru

Received July 2, 2010

Abstract—The $CuO–CeO_2/Al_2O_3$ catalysts for the selective oxidation of CO in hydrogen-containing mixtures were prepared by surface self-propagating thermal synthesis (SSTS) with the use of cerium nitrate $Ce(NO_3)_3$, the ammonia complex of copper acetate $[Cu(NH_3)_4](CH_3COO)_2$, and citric acid $C_6H_8O_7$ as a fuel additive. The effect of the $C_6H_8O_7/Ce(NO_3)_3$ molar ratio on the catalyst activity and selectivity for oxygen was studied. The catalyst samples were studied by X-ray diffraction (XRD) analysis, temperature-programmed reduction (TPR-H_2), IR spectroscopy of adsorbed CO, and transmission electron microscopy (TEM). It was found that an increase in the $C_6H_8O_7/Ce(NO_3)_3$ ratio resulted in an increase in the degree of dispersion of the resulting CeO_2 phase. The greatest amount of dispersed CuO particles, which are responsible for catalytic activity in the oxidation of CO, was formed at $C_6H_8O_7/Ce(NO_3)_3 = 1$.

DOI: 10.1134/S0023158411060012

INTRODUCTION

The problem of removing CO from hydrogen-rich gas mixtures is of considerable current interest for hydrogen power engineering. It is well known that systems based on palladium, ruthenium, and gold are effective catalysts for this process [1–5]. However, catalysts based on platinum group elements are insufficiently selective (in spite of high activity and stability at 150–250°C), and Au-containing catalysts, on which the oxidation of CO occurs at temperatures lower than 100°C, undergo deactivation by the reaction products CO_2 and H_2O. Furthermore, the widespread use of noble metals is limited because they are expensive. Oxide systems, in particular, $CuO–CeO_2$, are alternative to these catalysts. The oxidation of CO on these systems occurs at the interfaces of CuO and CeO_2; therefore, the activity of these systems depends on both the state of the CuO active centers and the redox ability of CeO_2, which makes it possible to reversibly add and eliminate oxygen in the course of reaction [6–10]. Various methods are used for the preparation of the $CuO–CeO_2$ catalysts: impregnation, coprecipitation, sol–gel method, etc. Previous studies [7, 11] showed that the method used for the preparation of $CuO–CeO_2$ affects the state and degree of dispersion of the phases, the degree of interaction between them, and, therefore, the catalytic properties. Among the methods of the preparation of bulk $CuO–CeO_2$ catalysts, the combustion method described in [12, 13] is of interest. This method makes it possible to obtain homogenized catalysts with high specific surface area and catalytic activity without the stage of calcination. The combustion method consists in the ignition of a mixture of $Cu(NO_3)_2$ and $Ce(NO_3)_3$ salts and urea as organic fuel under the action of a thermal pulse followed by self-sustaining combustion due to a redox reaction between the organic fuel and the mixture of salts. In this case, the characteristics of the resulting product, such as specific surface area, crystallite size, and catalytic properties, strongly depend on the amount of the fuel additive.

The surface self-propagating thermal synthesis (SSTS) of supported catalysts also belongs to methods in which combustion is used [14–17]. The SSTS consists in the self-propagating flameless combustion of active component precursors (without or with fuel additives) in a layer on the surface of a support. As a result, a sample with dispersed and imperfect active constituents on the support surface can be prepared in a short time (a few minutes).

The aim of this work was to study the $(CuO–CeO_2)/Al_2O_3$ supported catalysts prepared by SSTS in the reaction of the selective oxidation of CO in the presence of H_2, namely, to determine the effect of the fuel additive (citric acid) : cerium(III) nitrate ratio ($C_6H_8O_7/Ce(NO_3)_3$) on the SSTS parameters and the structure and catalytic properties of $(CuO–CeO_2)/Al_2O_3$.

EXPERIMENTAL

Catalyst Preparation

The samples of $(CuO–CeO_2)/Al_2O_3$ were prepared by SSTS. γ-Al_2O_3 (S_{sp} = 200 m^2/g) as spherical granules of size ~2 mm (ZAO Ryazanskii NPK), which were precalcined at 600°C for 4 h, was used as a support.

A solution of CeO_2 was used as the precursor of $Ce(NO_3)_3$, and a solution of $[Cu(NH_3)_4](CH_3COO)_2$ served as the precursor of CuO. On supporting CeO_2, a specified amount of citric acid ($C_6H_8O_7$), which served as a fuel additive, was added to the solution of $Ce(NO_3)_3$. Then, the samples were dried at a temperature of 120°C for 2 h. The components were supported step-by-step in the following order: (1) $Ce(NO_3)_3$ and (2) $[Cu(NH_3)_4](CH_3COO)_2$ with performing SSTS at either step. For this purpose, the granules of γ-Al_2O_3 with a supported component were placed in a reactor for SSTS [18] and thermostatically controlled at 80°C in a flow of air; then, a thermal pulse was given at the bottom end of the layer by a heated Nichrome coil (~700°C, to 30 s). As a result of this initiation, a solid-phase combustion front propagated through the sample layer and atmospheric oxygen served as an oxidizing agent. The temperature in the layer (in the front) was determined with the aid of a chromel–alumel thermocouple.

In the series of the prepared samples, the concentrations of CuO and CeO_2 were 7.5 and 15 wt %, respectively, and the $C_6H_8O_7/Ce(NO_3)_3$ molar ratio was varied in the range of 0.5–2. The samples are referred to as AMTs-*N*, where *N* is the varied molar ratio between citric acid and cerium nitrate. The reference sample, which was prepared by the impregnation of aluminum oxide with the solutions of $Ce(NO_3)_3$ and $Cu(CH_3COO)_2$ followed by calcination at 450°C (4 h), is referred to as AMTs-0.

Catalytic activity. The catalytic activity of the prepared samples in the reaction of CO oxidation in the presence of H_2 was determined in a flow system. The initial gas mixture contained 1% CO, 2% O_2, 8% N_2, and 89% H_2; its total flow rate was 10 ml/s at a contact time of 0.5 s. The concentrations of CO and O_2 before and after reaction were determined by chromatography (3-m column packed with zeolite CaA and a thermal conductivity detector). The catalyst was mixed with quartz to avoid overheating in the course of exothermic reactions. The temperature in the catalyst bed was controlled and regulated with the use of a chromel–alumel thermocouple connected to a Varta thermoregulator. In the course of the experiments, the temperature in the catalyst zone was increased from 90°C (with a step of 10°C); the sample was kept for 30–40 min at each temperature; in this time interval, four or five chromatographic analyses were performed to test the reproducibility of results.

The following equations were used in the calculations of the degrees of conversion of oxygen (X_{O_2}) and CO (X_{CO}) and the selectivity (S_{CO}), respectively:

$$X_{O_2} = \left[\left(P_{O_2}/P_{N_2}\right)_{irm} - \left(P_{O_2}/P_{N_2}\right)_{mar}\right]/\left(P_{O_2}/P_{N_2}\right)_{irm},$$

$$X_{CO} = [(P_{CO}/P_{N_2})_{irm} - (P_{CO}/P_{N_2})_{mar}]/(P_{CO}/P_{N_2})_{irm},$$

$$S_{CO} = 0.5X_{CO}/X_{O_2},$$

where P_{O_2}, P_{CO}, and P_{N_2} are the peak areas of oxygen, CO, and nitrogen, respectively; the peak area P_{N_2} was used as an internal standard; and the subscripts irm and mar refer to the initial reaction mixture and the mixture after the reactor, respectively.

X-ray diffraction analysis. The X-ray diffraction (XRD) analysis of the samples was carried out with the use of a D 8 Advance diffractometer (Bruker) in the monochromated CuK_α radiation. The particle (CSR) size of the supported phase of CeO_2 was calculated from the Selyakov–Scherrer formula.

Temperature-programmed reduction. Temperature-programmed reduction (TPR-H_2) was performed on an AutoChem II 2920 instrument in a mixture of 10% H_2/Ar at a flow rate of 25 ml/min. The rate of heating to 500°C was 10 K/min. Before performing the experiment, the sample was processed in a flow of Ar at 35°C for 30 min.

IR spectroscopy. The IR spectra of adsorbed CO molecules were recorded on an IR Prestige-21 spectrophotometer with a resolution of 4 cm^{-1} and a spectrum accumulation number of 50 at room or liquid-nitrogen temperature and a pressure of 10 Torr. The samples were pressed as pellets without a binding agent (the density of pellets is specified in Figs. 4 and 5) and evacuated for 1 h at 300°C to a residual pressure of ~10^{-4} Torr.

Electron microscopic studies. A JEM 2100 JEOL transmission electron microscope (accelerating voltage, 200 kV; crystal lattice resolution, 0.14 nm) was used to perform the electron-microscopic (TEM) studies. The samples were dispersed in an alcohol (ethanol) with the use of a UZDN-2T ultrasonic disperser and supported from the alcohol suspensions into copper gauze substrates. Interplanar spacing was determined from the direct image of a crystal lattice in electron micrographs, from electron diffraction patterns, and by rapid Fourier transform with the use of the Gatan DigitalMicrograph software package.

RESULTS AND DISCUSSION

Self-propagating thermal synthesis occurs under appropriate conditions, the most important of which is the sufficient release of heat on solid-phase flameless combustion. Fuel additives are used if heat consumption is required for converting active constituent precursors into active phases. These additives include

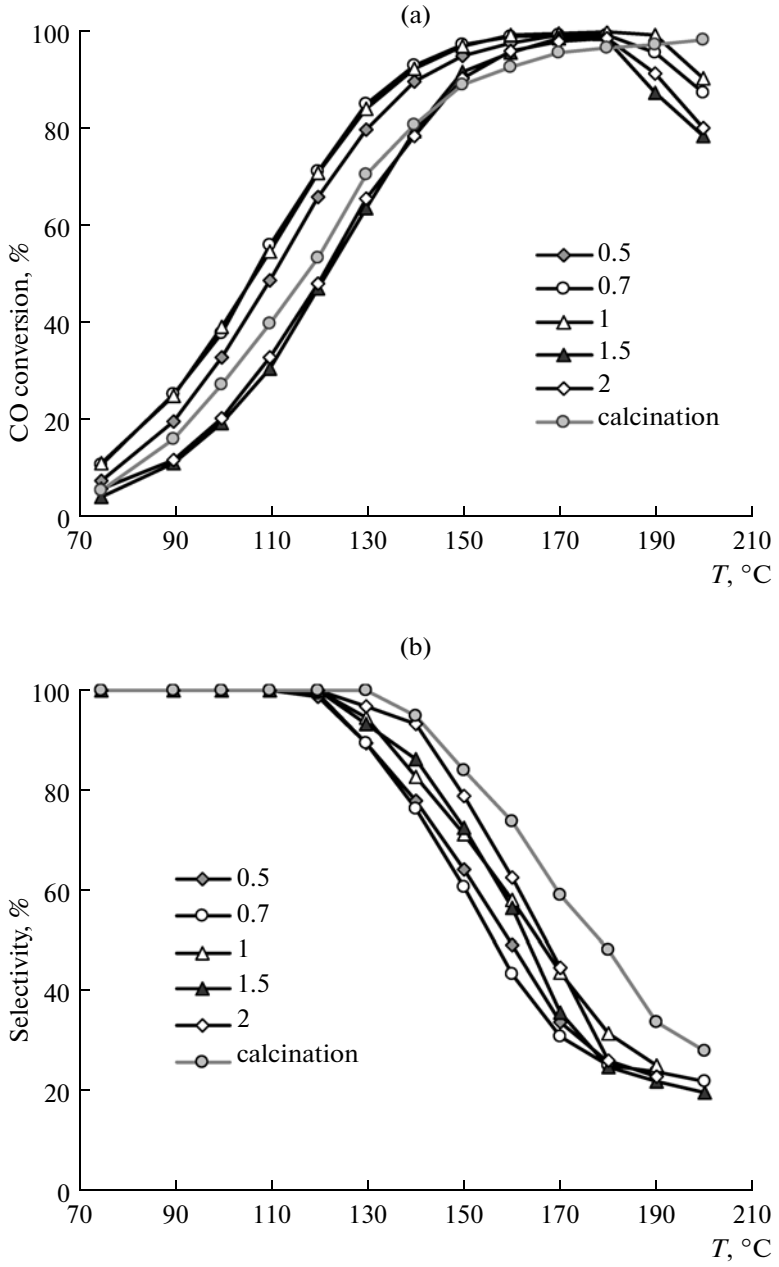

Fig. 1. The temperature dependence of (a) the CO conversion and (b) selectivity for AMTs catalysts with different N values.

substances the combustion of which generates heat sufficient for the decomposition of an active constituent precursor. In the case under consideration, citric acid served as this additive in the supporting of CeO_2 from $Ce(NO_3)_3$.

In the course of SSTS, we found that an increase in the amount of citric acid in a range (N) from 0.5 to 2 leads to an increase in the recorded temperature of a combustion front from 300 to 600°C and also to an increase in the speed of propagation of the combustion front through the sample layer from ~0.13 to 0.21 mm/s. Note that, at $N = 2$, SSTS occurs with the intense release of gases accompanied by the rupture of a considerable portion of granules.

After supporting CuO, the combustion front temperature of $[Cu(NH_3)_4](CH_3COO)_2$ (without the additive) was 453–513°C for all of the samples, and the speed of propagation of the combustion front was ~0.05 mm/s.

Catalytic Properties of $(CuO–CeO_2)/\gamma$-Al_2O_3

Figure 1 shows the results of the catalytic experiments carried out at 75–200°C. As can be seen, the

amount of citric acid used at the stage of supporting CeO_2 noticeably affects the catalytic activity of SSTS samples. The most active catalysts were prepared at $N = 0.7$ and 1. The dependences of the CO conversion on reaction temperature are almost the same; the activity of AMTs-0.5 is somewhat lower. For these samples, the maximum conversion of CO (98–99%) is achieved at a temperature of 160°C and remains unchanged up to 180°C or, in the case of AMTs-1, to 190°C. As the reaction temperature is further increased, the CO conversion decreases because of the occurrence of a competitive hydrogen oxidation reaction. According to published data [10], the rate of this reaction increases with temperature more strongly than the rate of CO oxidation because the activation energy of hydrogen oxidation is 142 kJ/mol, whereas $E_a = 94.4$ kJ/mol for the oxidation of CO.

The CO conversion curves are shifted toward the higher temperature region at $N > 1$. They almost coincide for AMTs-1.5 and AMTs-2 and reach a maximum value of 98–99% at 170–180°C.

Thus, the catalytic activity of the $(CuO–CeO_2)/Al_2O_3$ samples prepared by SSTS depends on the amount of citric acid, which is used at the stage of their preparation, and it reaches the greatest value at $N = 1$.

The selectivity of CO oxidation is 100% for all of the samples up to 120°C. At this temperature, the CO conversion is 71% in the case of AMTs-0.7 and AMTs-1; $X_{CO} = 65\%$ for AMTs-0.5 and $X_{CO} = 47–48\%$ for AMTs-1.5 and AMTs-2.

From a comparison of the catalytic properties of the most active AMTs-1 with the properties of AMTs-0, which was prepared by traditional calcination, it follows (Fig. 1) that the SSTS sample is more active than AMTs-0, but it is inferior to it in terms of selectivity. For AMTs-0, the CO conversion gradually increases as the reaction temperature is increased from 160°C and reaches 98–99% at 190–200°C.

The catalytic activity of copper–cerium catalysts depends on the degree of dispersion of CuO and CeO_2 particles. It is believed [13, 19, 20] that easily reducible fine particles (ions or clusters), which strongly interact with CeO_2 particles, are the active centers of CO oxidation. According to Liu and Stephanopoulos [21], this interaction leads to the stabilization of Cu^+ particles at the interface; unlike to bulk CuO, these particles can strongly adsorb CO, whereas CeO_2 serves as a source of oxygen. As the particle size of CuO increases, its interaction with CeO_2 becomes weaker and the catalytic activity decreases.

X-ray Diffraction Analysis

The diffraction patterns of samples prepared at different $C_6H_8O_7/Ce(NO_3)_3$ ratios exhibit reflections corresponding to CeO_2 and Al_2O_3 phases (Fig. 2). Peaks characteristic of the CuO phase are absent from the region of 35–39°, and only a gently sloping maximum due to γ-Al_2O_3 is observed. According to published data, the crystalline phase of CuO in the $CuO–CeO_2$ system is formed only above 800°C [22] or at the CuO content of ≥ 10 wt % [19, 20]. Therefore, the absence of the peak of CuO from the samples can be due to both the small particle size of CuO on the surface of CeO_2 and the formation of the solid solution $Cu_xCe_{1-x}O_{2-y}$ [23] or to a combination of these two factors.

The diffraction patterns of SSTS catalysts and the AMTs-0 sample are essentially different. In the latter sample, the peak of CeO_2 at 28° is narrow and is intense, whereas its noticeable broadening with increasing the ratio N is characteristic of SSTS samples. In this case, the size of primary CeO_2 particles varies from 7.0 to 3.0 nm, whereas their size is ~7.5 nm in AMTs-0. It is most likely that the smearing of peak observed with increasing the amount of the fuel additive is due to an increase in the degree of dispersion of CeO_2 particles in spite of an increase in the combustion front temperature on SSTS. It is likely that the time of thermal action rather than the thermal wave temperature on SSTS affects the formation of the CeO_2 phase; as noted above, this time increases with decreasing the amount of the fuel additive.

According to Martines-Aries et al. [24], at least two types of CeO_2 particles occur in the CeO_2/Al_2O_3 catalysts: fine (two-dimensional) particles, which strongly interact with the support and essentially differ from pure CeO_2 in their chemical behavior, and relatively large three-dimensional particles with properties similar to those of pure CeO_2. In this case, the catalytic activity Of $(CuO–CeO_2)/Al_2O_3$ in the oxidation of CO increases with the cerium content of the catalyst and, correspondingly, with the amount of three-dimensional particles. This allowed Martines-Aries et al. [24] to conclude that the catalytic activity of $(CuO–CeO_2)/Al_2O_3$ was caused by the interaction of copper with three-dimensional CeO_2 particles.

According to this point of view, the decrease in the catalytic activity of the $CuO–CeO_2/Al_2O_3$ samples prepared at $N > 1$ observed in this work can be explained by an increase in the degree of dispersion of the supported CeO_2 phase based on the results of XRD analysis; this strengthens the interaction of CeO_2 particles with the Al_2O_3 support and weakens the interaction with the phase of CuO.

Temperature-Programmed Reduction with Hydrogen

The TPR-H_2 method was used to determine the state of a copper oxide phase in SSTS samples, which

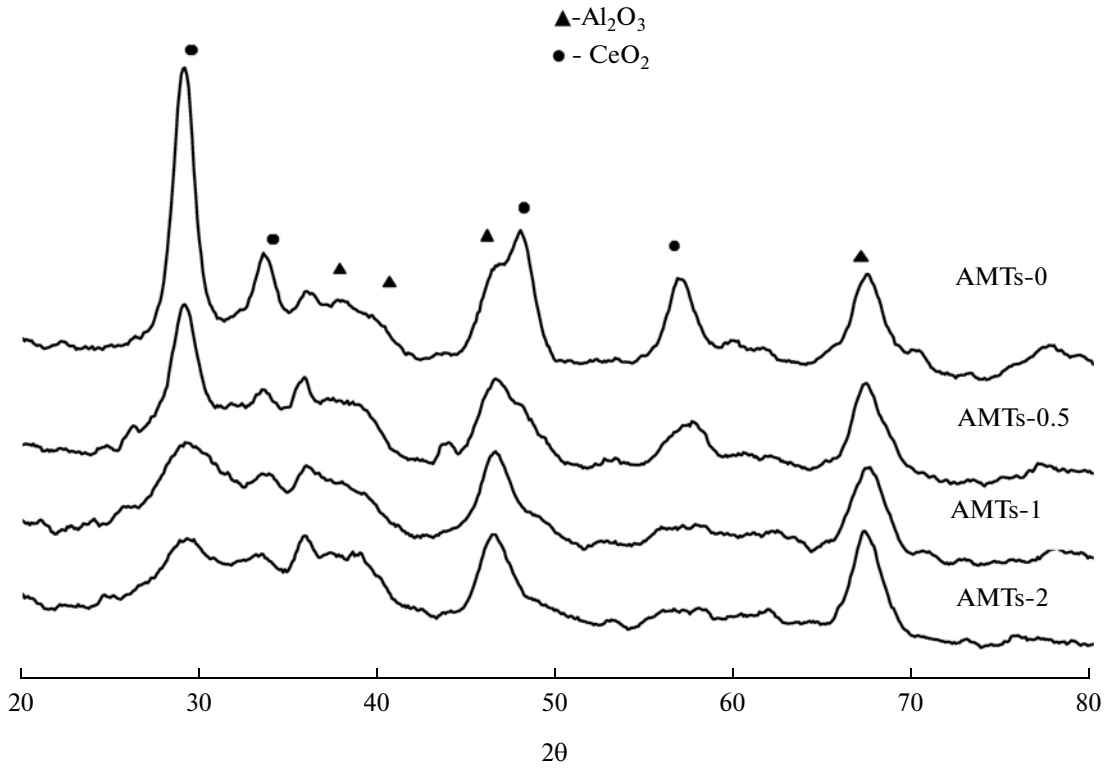

Fig. 2. Diffraction patterns of SSTS samples and the AMTs-0 sample prepared by calcination.

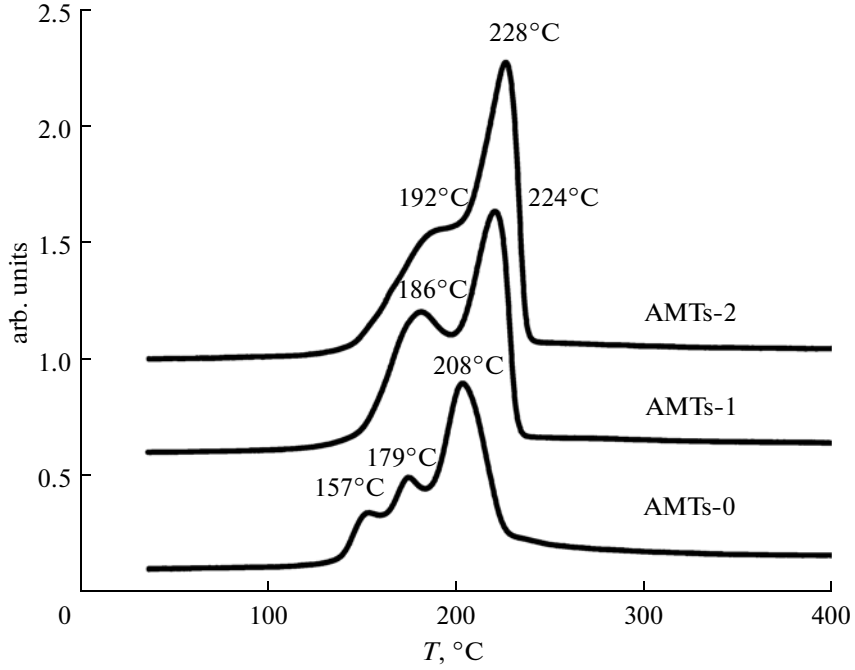

Fig. 3. TPR-H_2 curves for the AMTs-1, AMTs-2, and AMTs-0 samples.

exhibited high and low catalytic activity (AMTs-1 and AMTs-2), and AMTs-0; Fig. 3 shows the results.

According to published data [11, 25], the TPR-H_2 curves of copper–cerium systems are shifted toward low temperatures relative to the TPR-H_2 profile of pure CuO. This increase in reducing ability is caused by the interaction between copper oxide and oxygen vacancies on the surface of cerium oxide. The occurrence of this interaction is evidenced by the fact that, unlike the TPR-H_2 profile of pure CuO with one reduction peak, several peaks are characteristic of the

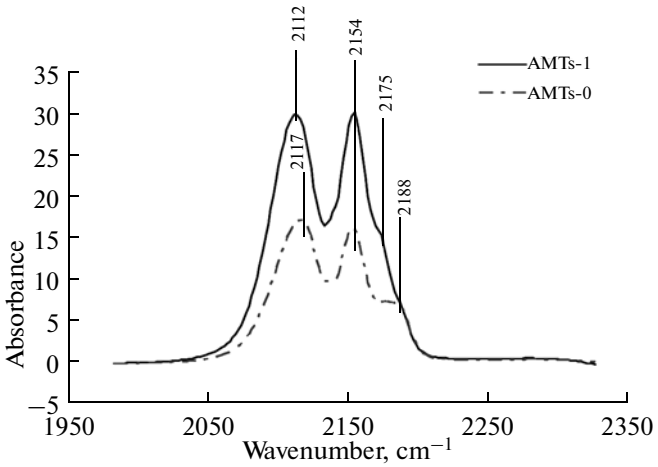

Fig. 4. IR spectra of adsorbed CO at a temperature of liquid nitrogen ($P = 10$ Torr) for the AMTs-1 ($\rho_{tab} = 24.98$ mg/cm^2) and AMTs-0 ($\rho_{tab} = 17.50$ mg/cm^2) samples.

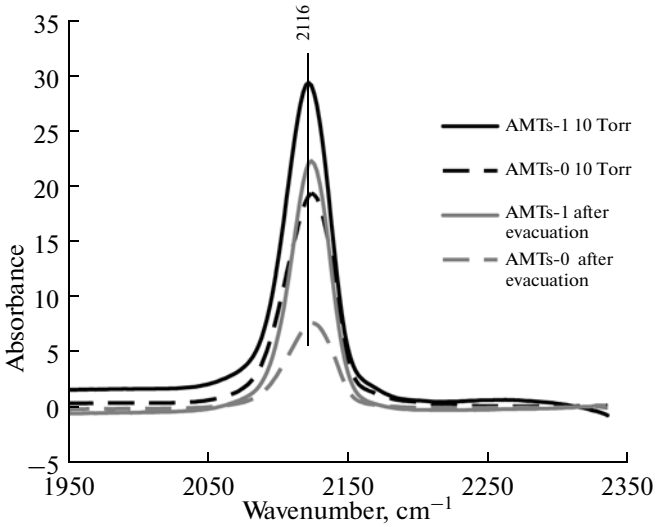

Fig. 5. IR spectra of adsorbed CO at room temperature for the AMTs-1 ($\rho_{tab} = 27.06$ mg/cm^2) and AMTs-0 ($\rho_{tab} = 29.91$ mg/cm^2) samples.

TPR-H_2 curves of the copper–cerium systems. This fact suggests the presence of CuO particles in different dispersed states, which are responsible for the degree of interaction between the oxides. Thus, for bulk CuO–CeO_2 oxides, a low-temperature peak in the TPR curve characterizes the reduction of uncrystallized fine CuO particles, which strongly interact with CeO_2 to stabilize Cu^+ particles at the interface. The peaks observed with a further increase in the temperature correspond to the reduction of larger CuO particles weakly associated with CeO_2 and the reduction of bulk crystalline CuO.

In our case, the reduction of SSTS samples occurs in two stages, which are characterized by peaks at 186 and 224°C for AMTs-1 and at 192 and 228°C for AMTs-2. In accordance with published data [11, 25], we believe that the peak at 186–192°C corresponds to fine CuO particles, which strongly interact with CeO_2; this interaction is responsible for the catalytic activity of these systems. For AMTs-1, this peak has a higher intensity at a lower reduction temperature than that in the case of AMTs-2; this is consistent with the results of catalytic experiences, which showed that AMTs-1 is more active than AMTs-2. The peak observed in SSTS samples at 224–228°C relates to the reduction of large CuO particles [11, 25]. However, in our case, we did not detect CuO crystals based on both the diffraction patterns and numerous electron-microscopic photographs (see below). Therefore, we can conclude that the second peak (224–228°C) is caused by the reduction of $Cu_xCe_{1-x}O_{2-y}$ particles.

Thus, the difference in the reduction profiles of SSTS samples, which differ only in cerium oxide particle sizes, suggests that the degree of dispersion of the CeO_2 phase influences the subsequent formation of dispersed CuO, which interacts with the CeO_2 phase and the $Cu_xCe_{1-x}O_{2-y}$ solid solution, and hence the catalytic activity.

The TPR profile for the AMTs-0 sample, which was prepared by calcination, is shifted toward low temperatures (as compared with the reduction curves for the SSTS catalysts), and it has three peaks at 157, 179, and 208°C. In accordance with published data, the first two peaks can be ascribed to the reduction of CuO particles strongly interacting with CeO_2. However, a peak at 208°C, which was attributed previously [11, 25] to the reduction of coarse CuO particles, is difficult to identify in our case because we failed to detect a phase of CuO in this sample by the techniques used in this study (XRD analysis and TEM). In spite of lower reduction temperatures, the intensities of the first two peaks are small in comparison with the peak for AMTs-1; this fact suggests a smaller amount of active centers, and it can be responsible for the lower catalytic activity.

IR Spectroscopy of Adsorbed CO

The IR spectra of adsorbed CO measured at a temperature of liquid nitrogen and a pressure of 10 Torr (Fig. 4) contain absorption bands with the maximums at 2112 and 2117 cm^{-1} for AMTs-1 and AMTs-0, respectively, which correspond to the molecular vibrations of CO adsorbed at theCu^{1+} centers [26, 27]. Both of the spectra also exhibit an absorption band at 2154 cm^{-1}, which cannot be unambiguously interpreted. According to published data [27, 28], the presence of this absorption band in the spectrum suggests the adsorption of CO at the Ce^{4+} centers. According to Tikhov et al. [29], this absorption band belongs to the molecular vibrations of CO adsorbed on copper oxides, for example, at a center like Cu^{1+}–O–Cu^{2+}–O–Cu^{1+}, where Cu^{2+} is the site of CO adsorption. The

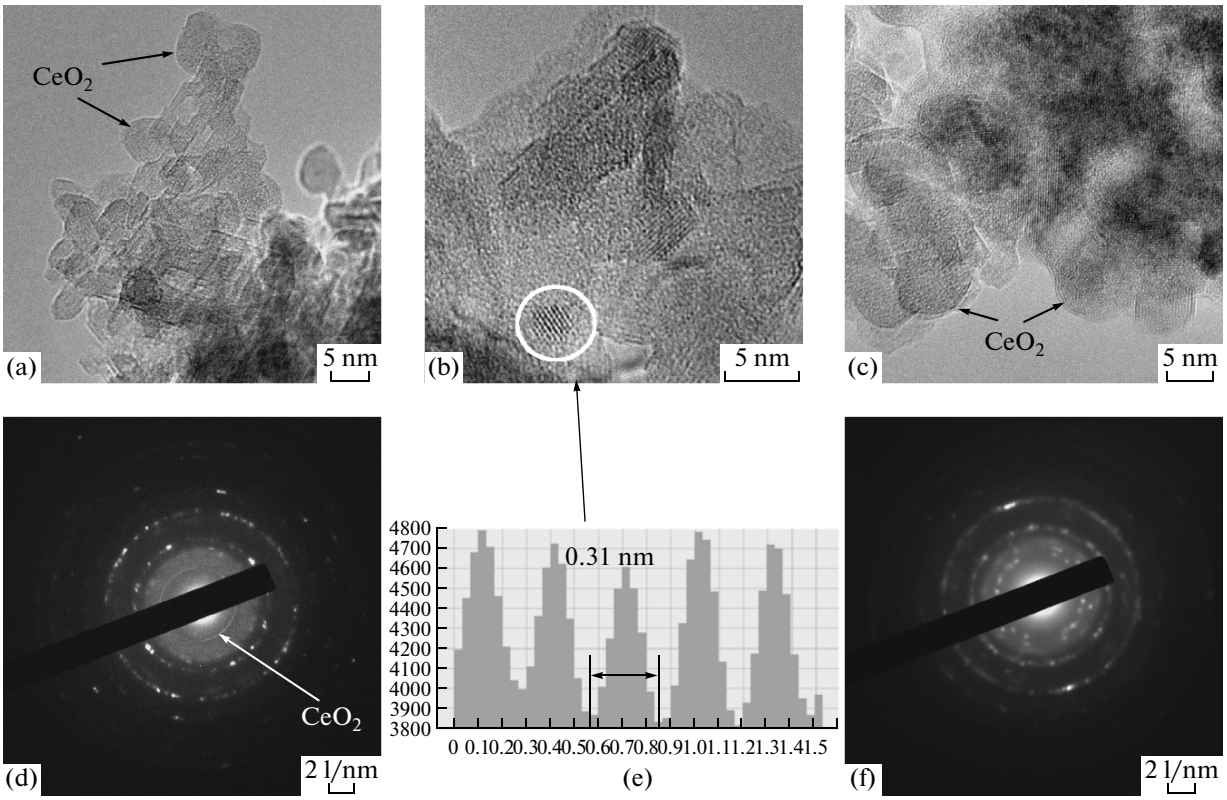

Fig. 6. (a, b) Electron micrographs, (d) electron diffraction pattern, and (e) contrast distribution profile for a particle marked with an arrow in the AMTs-2 sample. (c) Electron micrograph and (f) electron diffraction pattern of the AMTs-0 sample.

spectrum of AMTs-1 also contains an absorption band at 2175 cm^{-1}, which corresponds to vibrations of CO molecules adsorbed on the Cu^{2+} ions [29]. The presence of an absorption band at 2188 cm^{-1} in the spectra of both of the catalysts suggests that the samples contain weak Al^{3+} Lewis acid sites (LASs) [28]. This band in the spectrum of AMTs-0 is more intense than that in the spectrum of AMTs-1.

After the adsorption of CO at room temperature, only one absorption band with a maximum at 2116 cm^{-1} is observed in the IR spectra of both of the samples (Fig. 5). As noted above, this absorption band characterizes the presence of strong Cu^{1+} LASs; in this case, its intensity for the AMTs-1 sample is higher than for AMTs-0. After the evacuation of CO for 5 min, this peak shifts to 2119 cm^{-1} and its intensity decreases; this decrease in the AMTs-0 catalyst is greater than that in AMTs-1.

As can be seen, in all cases, the IR spectra of AMTs-1 are almost identical to the spectra of the AMTs-0 sample prepared by calcination; this fact suggests the same nature of CO adsorption centers. However, they are characterized by higher absorption band intensities for the SSTS sample. In our opinion, different absorption band intensities at the same active constituent concentrations in the samples were due to different concentrations of adsorption centers on the catalyst surface. It is likely that, upon the SSTS of catalysts, the distribution of not only cerium oxide (as follows from XRD data) but also copper oxide is more dispersed, as compared with traditional calcination.

Electron Microscopy

According to electron microscopic data, the samples synthesized by SSTS consist of primary particles with different morphologies and sizes. The crystallites of γ-Al_2O_3 are largely well crystallized, and they have a platelet shape and sizes of 5–10 nm. The particles of CeO_2 have a round shape without clear crystal faceting with sizes of 2–5 nm (Figs. 6a, 6b). The high-resolution micrographs exhibit crystal planes with periodicities of 0.26 and 0.31 nm (Figs. 6b, 6e), which are characteristic of the phase of CeO_2. In addition, note that the analysis of a large number of electron micrographs did not reveal the presence of the phase of CuO.

The electron diffraction patterns of these samples consist of several rings (or a set of reflections located in specific circles), the majority of which corresponds to the phase of γ-Al_2O_3 (di: 0.239, 0.198, and 0.139 nm; PDF 10-0425). In addition, there is a thin low-contrast ring (d 0.31 nm; PDF), which can belong to the phase of CeO_2 or to $Cu_xCe_{1-x}O_{2-y}$ (Fig. 6d). Many authors [9, 12, 23]

observed a decrease in the lattice parameter of CeO_2 upon supporting CuO, which suggests the possibility of the formation of the $Cu_xCe_{1-x}O_{2-y}$ solid solution; in their opinion, this confirms the replacement of cerium ions by Cu^{2+} ions in the matrix of CeO_2.

However, note that the electron diffraction patterns of AMTs-0 (Fig. 6f), which were obtained under the same operating conditions of the microscope as those for the samples synthesized by SSTS, exhibit only individual point reflections (without a change in the maximum intensity position) in place of a ring corresponding to the phase of CeO_2. This special feature suggests the presence of larger CeO_2 particles in this sample; this is supported by electron-microscopic photographs (particle sizes of 5–10 nm) (Fig. 6c) and correlate with the results of XRD analysis.

Thus, XRD analysis, TPR, IR-spectroscopic, and TEM data indicate that the use of SSTS for the synthesis of the catalytically active $CuO–CeO_2$ system supported on Al_2O_3 makes it possible to increase the degree of dispersion of CeO_2 and CuO particles, as compared with traditional calcination. This favorably affects the catalytic activity in the oxidation of CO with a correctly chosen amount of the fuel additive for SSTS. It is believed that the degree of dispersion and degree of interaction of CuO and CeO_2 phases can be regulated by choosing SSTS conditions for the synthesis of $CuO–CeO_2/Al_2O_3$ catalysts (the nature and amount of fuel additives) in order to obtain highly active catalysts for the oxidation of CO in the presence of hydrogen.

CONCLUSIONS

The $(CuO–CeO_2)/Al_2O_3$ supported catalysts, which are promising for the oxidation of CO, were prepared by SSTS.

The degree of dispersion of the phase of CeO_2 increases with increasing the amount of citric acid as a constituent of precursors for SSTS in the range of $C_6H_8O_7/Ce(NO_3)_3 = 0.5–2$.

The greatest amount of fine CuO particles, which are responsible for the catalytic activity in CO oxidation, in the $(CuO–CeO_2)\gamma\text{-}Al_2O_3$ system is formed at the molar ratio $C_6H_8O_7/Ce(NO_3)_3 = 1$.

ACKNOWLEDGMENTS

This work was supported by the Russian Foundation for Basic Research (project no. 08-03-00335-a).

REFERENCES

1. Korotkikh, O. and Farrauto, R., *Catal. Today*, 2000, vol. 62, p. 249.
2. Date, M. and Haruta, M., *J. Catal.*, 2001, vol. 201, p. 221.
3. Wolf, A. and Schuth, F., *Appl. Catal., A*, 2002, vol. 226, p. 1.
4. Snytnikov, P.V., Sobyanin, V.A., Belyaev, V.D., Tsyrulnikov, P.G., Shitova, N.B., and Shlyapin, D.A., *Appl. Catal., A*, 2003, vol. 239, no. 1.
5. Liu, Z.G., Zhou, R.X., and Zheng, X.M., *J. Mol. Catal. A: Chem.*, 2006, vol. 255, p. 103.
6. Liu, Y., Fu, Q., and Stephanopoulos, M.F., *Catal. Today*, 2004, vol. 93.
7. Liu, Zh., Zhou, R., and Zheng, X., *J. Mol. Catal. A: Chem.*, 2007, vol. 267, p. 137.
8. Gamarra, D., Belver, C., Fernandez-Garcia, M., and Martinez-Arias, A., *J. Am. Chem. Soc.*, 2007, vol. 129, p. 12064.
9. Snytnikov, P.V., Stadnichenko, A.I., Semin, G.L., Belyaev, V.D., Boronin, A.I., and Sobyanin, V.A., *Kinet. Catal.*, 2007, vol. 48, no. 3, p. 448.
10. Lee, H.C. and Kim, D.H., *Catal. Today*, 2008, vol. 132, p. 109.
11. Zheng, X., Zhang, X., Wang, X., and Wu, S., *React. Kinet. Catal. Lett.*, 2007, vol. 92, no. 2, p. 195.
12. Ribeiro, N.F.P., Souza, M.V.M., and Schmal, M., *J. Power Sources*, 2008, vol. 179, p. 329.
13. Avgouropoulos, G. and Ioannides, T., *Appl. Catal., A*, 2003, vol. 244, p. 155.
14. Zav'yalova, U.F., Barbashova, P.S., Lermontov, A.S., Shitova, N.B., Tret'yakov, V.F., Burdeinaya, T.N., Lunin, V.V., Drozdov, V.A., Yashnik, S.A., Ismagilov, Z.R., and Tsyrul'nikov, P.G., *Kinet. Catal.*, 2007, vol. 48, no. 1, p. 162.
15. RF Patent 2297279, 2005.
16. RF Patent 2234979, 2003.
17. RF Patent 2039601, 1993.
18. RF Patent 2284219, 2005.
19. Luo, M.-F., Zhong, Y.-J., Yuan, X.-X., and Zheng, X.-M., *Appl. Catal., A*, 1997, vol. 162, p. 121.
20. Lin, R., Luo, M.-F., Zhong, Y.-J., Yuan, X.-X., Liu, G.-Y., and Liu, W.-P., *Appl. Catal., A*, 2003, vol. 255, p. 331.
21. Liu, W. and Stephanopoulos, M.F., *J. Catal.,* 1995, vol. 153, p. 304.
22. Jung, C.R., Han, J., Nam, S.W., Lim, T.-H., Hong, S.-A., and Lee, H.-I., *Catal. Today*, 2004, vols. 93–95, p. 183.
23. Gomez-Cortes, A., Marquez, Y., Arenas-Alatorre, J., and Diaz, G., *Catal. Today*, 2008, vols. 133–135, p. 743.
24. Martines-Aries, A., Cataluna, R., Conesa, J.C., and Soria, J., *J. Phys. Chem. B*, 1998, vol. 102, p. 809.
25. Marino, F., Schonbrod, B., Moreno, M., Jobbagy, M., Baronetti, G., and Laborde, M., *Catal. Today*, 2008, vols. 133–135, p. 735.
26. Davydov, A.A., *IK-spektroskopiya v khimii poverkhnosti okislov* (IR Spectroscopy Applied to the Chemistry of Oxide Surfaces), Novosibirsk: Nauka, 1984.
27. Moretti, E., Lenarda, M., Storaro, L.., Talon, A., Frattini, R., Polizzi, S., Rodriguez-Castellon, E., and Jimenez-Lopez, A., *Appl. Catal., A*, 2008, vol. 335, p. 46.
28. Paukshtis, E.A., *Infrakrasnaya spektroskopiya v getero-gennom kislotno-osnovnom katalize* (IR Spectroscopy Applied to Heterogeneous Acid–Base Catalysis), Novosibirsk: Nauka, 1992, p. 102.
29. Tikhov, S.F., Sadykov, V.A., Kryukova, G.N., Paukshtis, E.A., Popovskii, V.V., Starostina, T.G., Kharlamov, G.V., Anufrienko, V.F., Poluboyarov, V.F., Razdobarov, V.A., Bulgakov, N.N., and Kalinkin, A.V., *J. Catal.*, 1992, vol. 134, p. 506.